The 1,3-diaryltriazenido(*p*-cymene)ruthenium(II) complexes with a high *in vitro* anticancer activity ☆

Jure Vajs [a],[1], Ivana Steiner [b],[1], Anamaria Brozovic [b],[1], Andrej Pevec [a], Andreja Ambriović-Ristov [b],
Marija Matković [c], Ivo Piantanida [c], Damijana Urankar [a], Maja Osmak [b],*, Janez Košmrlj [a],*

[a] *Faculty of Chemistry and Chemical Technology, University of Ljubljana, Večna pot 113, SI 1000, Ljubljana, Slovenia*
[b] *Division of Molecular Biology, Ruđer Bošković Institute, Bijenička cesta 54, HR-10000, Zagreb Croatia*
[c] *Division of Organic Chemistry and Biochemistry, Ruđer Bošković Institute, Bijenička cesta 54, HR-10000 Zagreb, Croatia*

ABSTRACT

1,3-Diaryltriazenes (**1**) were let to react with [RuCl$_2$(*p*-cymene)]$_2$ in the presence of trimethylamine to give neutral 1,3-diaryltriazenido(*p*-cymene)ruthenium(II) complexes, [RuCl(*p*-cymene)(ArNNNAr)] (**2**). The molecular composition of the products **2** was confirmed by NMR spectroscopy and mass spectrometry. The structures of the selected complexes were confirmed by a single crystal X-ray analysis. All triazenido-ruthenium complexes were highly cytotoxic against human cervical carcinoma HeLa cells with IC$_{50}$ below 6 μM, as determined by a spectrophotometric MTT (3-(4,5-dimethylthiazol-2-yl)-2,5-diphenyl-tetrazolium bromide) method. The most active was [RuCl(*p*-cymene)(ArNNNAr)] (Ar = 4-Cl-3-(CF$_3$)-C$_6$H$_3$) (**2g**) with IC$_{50}$ of 0.103 ± 0.006 μM. In comparison with the data for the non-coordinated triazenes **1**, the triazenido-ruthenium complexes **2** exhibited up to 560-times higher activity. Three selected complexes were highly cytotoxic also against several tumor cell lines: laryngeal carcinoma HEp-2 cells and their drug-resistant HEp-2 subline (7 T), colorectal carcinoma HCT-116 cells, lung adenocarcinoma H460 cells, and mammary carcinoma MDA-MB-435 cells. The compounds **2g** and [RuCl(*p*-cymene)(ArNNNAr)] (Ar = 4-I-C$_6$H$_4$) (**2j**) were similarly cytotoxic against parental and drug-resistant cells. Time and dose dependent accumulation of the cells in the S phase of the cell cycle was induced by the compound **2g**, triggering apoptosis. Our preliminary results indicate triazenido-ruthenium complexes as promising anticancer drug candidates.

© 2015 Elsevier Inc. All rights reserved.

1. Introduction

The discovery of antitumor properties of cisplatin in 1965 by Rosenberg and co-workers has been one of the major medicinal breakthroughs for the metal-based drugs, opening a new field of anticancer research based on metallo-pharmaceuticals [1]. Even though nowadays cisplatin and its analogues are widely used in a modern anticancer chemotherapy, these compounds display several unwanted effects including high toxicity and development of the drug-resistance [2–4]. Therefore, there is an urge to investigate new alternative chemotherapeutic agents. Out of the metals that have been probed for the metal-based anticancer therapies, the ruthenium is one of the most promising [5–10]. Besides possessing rich potential in coordination chemistry [11], its complexes generally show low toxicity and the ability to mimic iron atoms in some cases. Because the fast dividing cancer cells have higher affinity to iron, they are easily reached by the ruthenium compounds accumulating more in the tumor than in the normal cells [12,13]. To date, two ruthenium complexes, NAMI-A and KP1019, have entered human clinical trials [5,9,10].

1,3-Diaryltriazenes have been broadly investigated for their pharmaceutical potential. In addition to the reports on their antibacterial [14] and antifungal [15] activity, their most widespread use is in the development of novel anticancer molecules [16–19]. In some cases, their mode of action is related to the methylation of DNA, leading to a somatic point mutation represented by C:G → T:A transition in DNA helix, and finally to the cell death [20].

It has been well accepted that a synergistic effect can arise from the combination of two pharmacophores into a single compound [21,22], which prompted us to combine cymene-ruthenium and 1,3-diaryltriazenes entities into the corresponding triazenido-ruthenium complexes to be screened for a cytotoxic activity against human cancer cell lines. Surprisingly, although the synthesis and reactivity of the triazenido complexes with ruthenium [23–27], as well as osmium [23,25], palladium [28,29], rhodium [30], platinum [31], aluminium [32], gallium [32], some heavier alkaline earths [33], and other metals [34] is precedented, to our knowledge no biological properties of such compounds have been reported to date.

---

2. Experimental section

2.1. Physical measurements

Melting points were determined on a Kofler micro hot stage apparatus and are uncorrected. NMR spectra were recorded at 23 °C with a Bruker Avance III 500 spectrometer (^{1}H NMR spectra at 500 MHz; ^{13}C NMR spectra at 126 MHz). Proton spectra are referenced to TMS as an internal standard; the carbon chemical shifts are given against the central line of the solvent signal ($CDCl_3$ at $\delta = 77.0$ ppm). IR spectra were obtained with a Bruker ALPHA Platinum ATR spectrometer on a solid sample support (ATR). High resolution mass spectrometry (HRMS) analyses were performed using an Agilent 6224 Accurate Mass TOF LC/MS spectrometer. Elemental analyses (C, H, N) were performed with Perkin Elmer 2400 Series II CHNS/O Analyser. TG/DSC measurements were performed on a Metter Toledo TGA/DSC1 Instrument. UV–Vis measurements were performed on UV/vis spectrometer Varian Cary 100 Bio while the CD experiments were performed on Circular Dichroism Spectrometer Jasco J-815.

2.2. X-ray crystal structure determination

Crystal data and refinement parameters of the compounds **2e** and **2h** are listed in Table S1. The X-ray intensity data were collected at room temperature with an Agilent SuperNova dual source with an Atlas detector equipped with mirror-monochromated Mo-K_α radiation ($\lambda = 0.71073$ Å) for **2e** and with a Nonius Kappa CCD diffractometer equipped with graphite-monochromated Mo-K_α radiation ($\lambda = 0.71073$ Å) for **2h**. The data were processed using CRYSALIS PRO [35] (**2e**) or DENZO [36] (**2h**). Both structures were solved by direct methods using SIR-92 [37] (**2e**) or SHELXS-97 [38] (**2h**) and refined against F^2 on all data by a full-matrix least squares procedure with SHELXL-97 [38]. All non-hydrogen atoms were refined anisotropically. All hydrogen atoms were included in the model at geometrically calculated positions and refined using a riding model. The fluorine atoms of CF_3 substituent and methine C13 atom in **2e** are disordered over two orientations and were modelled with split positions, with the use of PART instruction. Selected bond lengths and angles for **2e** and **2h** are listed in Table 1. Crystallographic data for structures have been deposited at the Cambridge Crystallographic Data Centre as supplementary publication CCDC 1063947 (**2e**) and 1063948 (**2h**). Copies of the structures can be obtained free of charge from The Cambridge Crystallographic Data Centre via www.ccdc.cam.ac.uk/data_request/cif.

Table 1
Selected bond lengths (Å) and angles (°) for **2e** and **2h**.

	2e	2h
Ru1–Cl1	2.3788(8)	2.3942(16)
Ru1–N1	2.1088(18)	2.092(4)
Ru1–N3		2.080(4)
N1–N2	1.308(2)	1.323(5)
N2–N3		1.313(5)
N1–C1	1.404(3)	1.396(6)
N3–C8		1.409(6)
Ru1–N1–N2	97.50(13)	99.2(3)
Ru1–N1–C1	142.15(14)	140.8(3)
Ru1–N3–N2		100.2(3)
Ru1–N3–C8		141.0(3)
Cl1–Ru1–N1	83.20(5)	85.14(13)
Cl1–Ru1–N3		84.87(13)
N1–Ru1–N1[i]	58.87(10)	
N1–Ru1–N3		58.71(15)
N1–N2–N1[i]	104.8(2)	
N1–N2–N3		101.7(4)
C1–N1–N2	114.26(17)	119.2(4)
C8–N3–N2		118.6(4)

Symmetry code: (i) $x, -1.5-y, z$.

2.3. Reagents and materials

Starting materials and solvents for the synthesis of the examined compounds were used as obtained without further purification from the commercial sources. 1,3-Diaryltriazenes **1b** [14], **1c** [14], **1d** [18], **1e** [14], **1f** [39], **1g** [39], **1h** [14], **1i** [14], **1j** [39], **1k** [40] were prepared as described earlier. The progress of all reactions was monitored on Fluka silica-gel TLC-plates (with fluorescence indicator UV254) using ethyl acetate/petroleum ether (v/v 2:1) as the solvent system. A column chromatography was performed with Merck silica gel 60 (35–70 μm) with the solvent mixtures specified in the corresponding experiment.

2.4. Synthesis

2.4.1. General procedure for the synthesis of the complexes 2

To a stirred suspension of $[RuCl_2(\eta^6\text{-}p\text{-cymene})]_2$ (61.2 mg, 0.1 mmol) in methanol (20 mL), 1,3-diaryltriazene **1** (0.2 mmol) and triethylamine (558.0 μL, 0.4 mmol) were added. The reaction mixture was stirred for 0.5 h at room temperature. The product was precipitated by the addition of water (30 mL) and collected by filtration, yielding the corresponding complex **2**.

In the case of the complexes **2b**, **2d** and **2k**, the products were purified with a column chromatography using silica gel and petroleum ether/ethyl acetate (v/v 4:1) as the eluting solvent.

2.4.1.A. Complex 2a. Orange solid; yield 80%; mp 217–219 °C (MeOH/ H_2O); IR (cm^{-1}): 3018, 2963, 2865, 1947, 1588, 1478, 1456, 1385, 1369, 1324; ^{1}H NMR (500 MHz, $CDCl_3$): δ (ppm) 1.22 (d, $J = 6.9$ Hz, 6H), 2.34 (s, 3H), 2.77 (sep, $J = 6.9$ Hz, 1H), 5.37 (d, $J = 5.9$ Hz, 2H), 5.78 (d, $J = 5.9$ Hz, 2H), 7.05–7.11 (m, 2H), 7.28–7.36 (m, 8H); ^{13}C NMR (126 MHz, $CDCl_3$): δ (ppm) 19.2, 22.7, 31.7, 79.2, 81.4, 102.5, 102.6, 117.0, 124.3, 128.8, 147.0; HRMS (ESI+) for $C_{22}H_{24}N_3Ru$ [M–Cl]+: calcd 432.1014, found 432.1014. Anal. for $C_{22}H_{24}ClN_3Ru$: C, 56.59; H, 5.18; N, 9.00; found: C, 56.56; H, 4.90; N, 8.98.

2.4.1.B. Complex 2b. Orange solid; yield 88%; mp 168–170 °C (petroleum ether); IR (cm^{-1}): 3039, 2969, 2101, 2014, 1969, 1935, 1618, 1584, 1475; ^{1}H NMR (500 MHz, $CDCl_3$): δ (ppm) 1.30 (d, $J = 6.9$ Hz, 6H), 2.32 (s, 3H), 2.97 (sep, $J = 6.9$ Hz, 1H), 5.27 (d, $J = 5.8$ Hz, 2H), 5.82 (d, $J = 5.8$ Hz, 2H), 7.10–7.16 (m, 2H), 7.36–7.42 (m, 2H), 7.49–7.54 (m, 2H); ^{13}C NMR (126 MHz, $CDCl_3$): δ (ppm) 19.3, 22.7, 31.7, 78.5, 82.7 (d, $J = 5$ Hz), 102.5, 103.0, 119.4 (dq, $J_1 = 32$ Hz, $J_2 = 11$ Hz), 122.6 (q, $J = 273$ Hz), 123.0 (q, $J = 5$ Hz), 124.0 (d, $J = 4$ Hz), 124.9, 136.8 (d, $J = 8$ Hz), 151.5 (dq, $J_1 = 258$ Hz, $J_2 = 2$ Hz); HRMS (ESI+) for $C_{24}H_{20}F_8N_3Ru$ [M–Cl]+: calcd 604.0573, found 604.0575. Anal. for $C_{24}H_{20}ClF_8N_3Ru$: C, 45.12; H, 3.15; N, 6.58; found: C, 45.05; H, 2.78; N, 6.50.

2.4.1.C. Complex 2c. Yellow solid; yield 74%, mp 162–163 °C (MeOH/ H_2O); IR (cm^{-1}): 3359, 3070, 2967, 2033, 1615, 1524, 1485, 1451, 1425, 1375; ^{1}H NMR (500 MHz, $CDCl_3$): δ (ppm) 1.19 (d, $J = 6.9$ Hz, 6H), 2.14 (s, 3H), 2.75 (sep, $J = 6.9$ Hz, 1H), 5.30 (d, $J = 5.8$ Hz, 2H), 5.58 (d, $J = 5.8$ Hz, 2H), 7.13–7.21 (m, 2H), 7.31–7.38 (m, 2H), 7.43–7.52 (m, 2H); ^{13}C NMR (126 MHz, $CDCl_3$): δ (ppm) 18.9, 22.3, 31.2, 80.2, 82.4, 98.3, 102.9, 114.1 (dq, $J_1 = 20$ Hz, $J_2 = 3$ Hz), 119.2 (d, $J = 22$ Hz), 123.1 (qd, $J_1 = 273$ Hz, $J_2 = 2$ Hz), 124.3 (qd, $J_1 = 32$ Hz, $J_2 = 8$ Hz), 128.6 (d, $J = 8$ Hz), 142.4 (d, $J = 3$ Hz), 160.0 (d, $J = 247$ Hz); HRMS (ESI+) for $C_{24}H_{20}F_8N_3Ru$ [M–Cl]+: calcd 604.0573, found 604.0570. Anal. for $C_{24}H_{20}ClF_8N_3Ru$: C, 45.12; H, 3.15; N, 6.58; found: C, 44.81; H, 2.92; N, 6.67.

2.4.1.D. Complex 2d. Yellow-green solid; yield 78%; mp 55–57 °C (MeOH/ H_2O); IR (cm^{-1}): 2966, 2146, 2064, 2008, 1598, 1568, 1475, 1409, 1364, 1309; ^{1}H NMR (500 MHz, $CDCl_3$): δ (ppm) 1.21 (d, $J = 6.9$ Hz, 6H), 2.18 (s, 3H), 2.76 (sep, $J = 6.9$ Hz, 1H), 5.30 (d, $J = 5.9$ Hz, 2H), 5.59 (d, $J = 5.9$ Hz, 2H), 7.35–7.46 (m, 4H), 7.60–7.66 (m, 2H); ^{13}C NMR

(126 MHz, CDCl$_3$): δ (ppm) 19.0, 22.3, 31.4, 80.3, 82.0, 98.8, 103.2, 123.1 (q, J = 274 Hz), 123.8 (q, J = 32 Hz), 127.1, 127.9, 131.4, 132.4, 144.6; HRMS (ESI+) for C$_{24}$H$_{20}$Cl$_2$F$_6$N$_3$Ru [M−Cl]$^+$: calcd 635.9982, found 635.9978. Anal. for C$_{24}$H$_{20}$Cl$_3$F$_6$N$_3$Ru: C, 42.90; H, 3.00; N, 6.25; found: C, 43.29; H, 2.60; N, 6.18.

2.4.1.E. Complex 2e. Yellow solid; yield 61%; mp 201–203 °C (MeOH/H$_2$O); IR (cm^{-1}): 3053, 2967, 2103, 1979, 1898, 1603, 1514, 1477, 1416, 1388; ^{1}H NMR (500 MHz, CDCl$_3$): δ (ppm) 1.30 (d, J = 6.9 Hz, 6H), 2.33 (s, 3H), 2.90 (sep, J = 6.9 Hz, 1H), 5.24 (d, J = 5.9 Hz, 2H), 5.78 (d, J = 5.9 Hz, 2H), 7.17–7.25 (m, 2H), 7.34–7.41 (m, 2H), 7.64–7.70 (m, 2H); ^{13}C NMR (126 MHz, CDCl$_3$): δ (ppm) 19.3, 22.7, 31.8, 78.6, 82.7 (d, J = 5 Hz), 102.9, 103.3, 117.1 (d, J = 21 Hz), 117.7 (m), 112.9 (m), 123.5 (q, J = 272 Hz), 127.1 (qd, J$_1$ = 33 Hz, J$_2$ = 3 Hz), 135.8 (d, J = 9 Hz), 155.32 (d, J = 254 Hz); HRMS (ESI+) for C$_{24}$H$_{20}$F$_8$N$_3$Ru [M−Cl]$^+$: calcd 604.0573, found 604.0571. Anal. for C$_{24}$H$_{20}$ClF$_8$N$_3$Ru: C, 45.12; H, 3.15; N, 6.58; found: C, 45.02; H, 2.94; N, 6.49.

2.4.1.F. Complex 2f. Ocher solid; yield 83%; mp 191–193 °C (MeOH/H$_2$O); IR (cm^{-1}): 3060, 2969, 2872, 2103, 1912, 1594, 1483, 1417, 1384, 1305; ^{1}H NMR (500 MHz, CDCl$_3$): δ (ppm) 1.25 (d, J = 6.9 Hz, 6H), 2.35 (s, 3H), 2.78 (sep, J = 6.9 Hz, 1H), 5.37 (d, J = 5.9 Hz, 2H), 5.78 (d, J = 5.9 Hz, 2H), 7.05–7.18 (m, 4H), 7.31–7.38 (m, 2H); ^{13}C NMR (126 MHz, CDCl$_3$): δ (ppm) 19.3, 22.7, 31.9, 79.1, 81.5, 102.9, 103.1, 116.6, 116.8 (d, J = 14 Hz), 118.6, 121.4 (d, J = 19 Hz), 143.7 (d, J = 3 Hz), 155.5 (d, J = 246 Hz); HRMS (ESI+) for C$_{22}$H$_{20}$Cl$_2$F$_2$N$_3$Ru [M−Cl]$^+$: calcd 536.0046, found 536.0038. Anal. for C$_{22}$H$_{20}$Cl$_3$F$_2$N$_3$Ru: C, 46.21; H, 3.53; N, 7.35; found: C, 46.25; H, 3.23; N, 6.97.

2.4.1.G. Complex 2g. Yellow solid; yield 82%; mp 214–216 °C (diethyl ether/diisopropyl ether); IR (cm^{-1}): 3037, 2968, 2115, 1576 1474, 1424, 1388, 1366, 1317, 1304; ^{1}H NMR (500 MHz, CDCl$_3$): δ (ppm) 1.25 (d, J = 6.8 Hz, 6H), 2.36 (s, 3H), 2.79 (sep, J = 6.8 Hz, 1H), 5.42 (d, J = 6.0 Hz, 2H), 5.78 (d, J = 6.0 Hz, 2H), 7.40–7.46 (m, 4H), 7.56–7.60 (m, 2H); ^{13}C NMR (126 MHz, CDCl$_3$): δ (ppm) 19.3, 22.7, 31.9, 79.6, 81.4, 102.3, 103.8, 116.5 (q, J = 5 Hz), 120.5, 122.6 (q, J = 274 Hz), 127.6 (q, J = 2 Hz), 128.9 (q, J = 32 Hz), 132.0, 145.2; HRMS (ESI+) for C$_{24}$H$_{20}$Cl$_2$F$_6$N$_3$Ru [M−Cl]$^+$: calcd 635.9982, found 635.9984. Anal. for C$_{24}$H$_{20}$Cl$_3$F$_6$N$_3$Ru: C, 42.90; H, 3.00; N, 6.25; found: C, 43.30; H, 2.67; N, 6.27.

2.4.1.H. Complex 2h. Red solid; yield 91%; mp 222–224 °C (MeOH/H$_2$O); IR (cm^{-1}): 3076, 2968, 1608, 1575, 1541, 1525, 1486, 1431, 1371, 1311; ^{1}H NMR (500 MHz, CDCl$_3$): δ (ppm) 1.28 (d, J = 6.9 Hz, 6H), 2.40 (s, 3H), 2.81 (sep, J = 6.9 Hz, 1H), 5.51 (d, J = 6.0 Hz, 2H), 5.83 (d, J = 6.0 Hz, 2H), 7.59–7.63 (m, 2H), 7.70–7.73 (m, 2H), 8.01–8.06 (m, 2H); ^{13}C NMR (126 MHz, CDCl$_3$): δ (ppm) 19.4, 22.7, 32.0, 79.8, 81.5, 102.8, 104.9, 117.0 (q, J = 6 Hz), 120.0, 121.8 (q, J = 274 Hz), 125.7 (q, J = 34 Hz), 127.4, 144.1, 149.5; HRMS (ESI+) for C$_{24}$H$_{20}$F$_6$N$_5$O$_4$Ru [M−Cl]$^+$: calcd 658.0463, found 658.0466. Anal. for C$_{24}$H$_{20}$ClF$_6$N$_5$O$_4$Ru: C, 41.60; H, 2.91; N, 10.11; found: C, 41.88; H, 2.63; N, 10.04.

2.4.1.I. Complex 2i. Red solid; yield 80%; mp 231–233 °C (MeOH/H$_2$O); IR (cm^{-1}): 3050, 2970, 2225, 1598, 1567, 1491, 1438, 1382, 1316, 1274; ^{1}H NMR (500 MHz, CDCl$_3$): δ (ppm) 1.26 (d, J = 6.9 Hz, 6H), 2.39 (s, 3H), 2.80 (sep, J = 6.9 Hz, 1H), 5.50 (d, J = 6.0 Hz, 2H), 5.83 (d, J = 6.0 Hz, 2H), 7.54–7.59 (m, 2H), 7.67–7.71 (m, 2H), 7.78–7.83 (m, 2H); ^{13}C NMR (126 MHz, CDCl$_3$): δ (ppm) 19.4, 22.6, 32.0, 79.6, 81.5, 103.0, 104.8, 105.5 (q, J = 2 Hz), 115.6, 115.7 (q, J = 5 Hz), 120.0, 122.1 (q, J = 274 Hz), 134.1 (q, J = 33 Hz), 135.9, 149.3; HRMS (ESI+) for C$_{26}$H$_{20}$F$_6$N$_5$Ru [M−Cl]$^−$: calcd 618.0668, found 618.0661. Anal. for C$_{26}$H$_{20}$ClF$_6$N$_5$Ru: C, 47.82; H, 3.09; N, 10.73; found: C, 47.80; H, 2.86; N, 10.64.

2.4.1.J. Complex 2j. Ocher solid; yield 74%; mp 229–231 °C (MeOH/H$_2$O); IR (cm^{-1}): 2968, 2014, 1892, 1576, 1473, 1408, 1384, 1369, 1288, 1271; ^{1}H NMR (500 MHz, CDCl$_3$): δ (ppm) 1.21 (d, J = 6.9 Hz, 6H), 2.33 (s, 3H), 2.74 (sep, J = 6.9 Hz, 1H), 5.34 (d, J = 5.8 Hz, 2H), 5.75 (d, J = 5.8 Hz, 2H), 7.02–7.10 (m, 4H), 7.57–7.64 (m, 4H); ^{13}C NMR (126 MHz, CDCl$_3$): δ (ppm) 19.3, 22.7, 31.8, 79.1, 81.4, 88.1, 102.8, 102.9, 119.0, 137.8, 146.5; HRMS (ESI+) for C$_{22}$H$_{22}$I$_2$N$_3$Ru [M−Cl]$^+$: calcd 683.8947, found 683.8946. Anal. for C$_{22}$H$_{22}$ClI$_2$N$_3$Ru: C, 36.76; H, 3.09; N, 5.85; found: C, 37.01; H, 2.79; N, 5.99.

2.4.1.K. Complex 2k. Brown solid; yield 42%; mp 138.1–140.1 °C (diethyl ether); IR (cm^{-1}): 3068, 2834, 1604, 1580, 1496, 1458, 1440, 1357 1319, 1302; ^{1}H NMR (500 MHz, CDCl$_3$): δ (ppm) 1.23 (d, J = 6.9 Hz, 6H), 2.33 (s, 3H), 2.78 (sep, J = 6.9 Hz, 1H), 3.80 (s, 6H), 5.32 (d, J = 5.8 Hz, 2H), 5.75 (d, J = 5.8 Hz, 2H), 6.81–6.88 (m, 4H), 7.20–7.26 (m, 4H); ^{13}C NMR (126 MHz, CDCl$_3$): δ (ppm) 19.2, 22.7, 31.8, 55.6, 79.1, 81.4, 102.1, 102.3, 114.2, 118.0, 141.4, 156.6; HRMS (ESI+) for C$_{24}$H$_{28}$N$_3$O$_2$Ru [M−Cl]$^+$: calcd 492.1225, found 492.1225. Anal. for C$_{24}$H$_{28}$ClN$_3$O$_2$Ru: C, 54.70; H, 5.36; N, 7.97; found: C, 54.95; H, 5.10; N, 7.97.

2.5. Biology

2.5.1. Cell culture

Human cervical carcinoma HeLa and laryngeal carcinoma HEp-2 cells were obtained from the cell culture bank (GIBCO/Life Technologies, Grand Island, NY, USA). The development of the HEp-2 subline resistant to carboplatin has been published previously [41]. These cells are cross-resistant to the anticancer drugs cisplatin, transplatin and mitomycine C, as well as natural compound curcumin [41–43]. Large-cell lung carcinoma H460 cells, colorectal carcinoma HCT 116 and mammary carcinoma MDA-MB-435 cells [44] were obtained from American Type Culture Collection (ATCC; Manassas, VA, USA). All cell lines were grown as a monolayer culture in Dulbecco's modified Eagle's medium (DMEM; Sigma-Aldrich, St. Louis, MO, USA), supplemented with 10% foetal bovine serum (FBS; Sigma-Aldrich) in a humidified atmosphere of 5% CO$_2$ at 37 °C and were sub-cultured every 3–4 days.

2.5.2. Cytotoxicity assay

A cytotoxic activity of the triazenido-ruthenium complexes **2** was determined by MTT assay [45], modified as described. The cells were seeded into 96-well tissue culture plates (3000 cells/0.18 mL medium/well). The next day different concentrations of the complexes **2** were added (0.02 mL) to each well and each concentration was tested in quadruplicate. Following 72 h incubation at 37 °C, the medium was aspirated and 20 μg of 3-(4,5-dimethylthiazol-2-yl)-2,5-diphenyltetrazolium bromide (MTT) dye (Sigma-Aldrich) /0.04 mL medium/well was added. Three h later, formazan crystals were dissolved in DMSO (0.17 mL/well), the plates were mechanically agitated for 5 min and the optical density at 545 nm was determined on a microtiter plate reader (Awareness Technology Inc., Palm City, FL, USA). Each experiment was repeated at least three times. The same protocol was used to determine the cytotoxic activity of triazenes **1c** and **1j**.

2.5.3. Cell cycle analysis

Human cervical carcinoma HeLa cells were seeded into 6-well tissue culture plates (100,000 cells/2 mL medium/well). Next day they were treated with concentrations of **2g** that reduced the cell survival to 60 or 10% (survival fraction 0.6 and 0.1). After 24 and 48 h both adherent and floating cells were collected, washed with PBS and fixed overnight in 96% ethanol at −20 °C. Fixed cells were treated with RNase A (0.1 mg/mL; Sigma-Aldrich) for 1 h at room temperature and afterward stained with propidium iodide (50 μg/mL; Sigma-Aldrich) for 30 min in the dark. The DNA content was analysed by a flow cytometry (FACS Calibur, Becton Dickinson, Mountain View, CA, USA). The data were

analysed with the ModFitLTTM program (Verity Software House Inc., Topsham, ME, USA).

2.5.4. Western blot analysis

The western blot analysis was used for the determination of a poly (ADP-ribose) polymerase (PARP) cleavage as one of the markers for the apoptosis induction [46]. Upon treatment of the HeLa cells during 24 and 48 h with two concentrations of **2g** (IC_{40} and IC_{90}) the adherent and floating cells were collected and protein isolation was performed following the previously used protocol [43]. 30 mg of the total cellular proteins were loaded onto a 10% SDS polyacrylamide gel and run for 2 h at 35 mA in a Mini-PROTEAN Tetra cell system (Bio-Rad, Hercules, CA, USA). The separated proteins were transferred onto a 0.2 mm nitro-cellulose membrane (Schleicher & Schuell, Dassel, Germany; Cat. Nr. NBA083C001EA) by using the same Bio-Rad system optimised for a pro-tein transfer with a Mini Trans-Blot® Module (Bio-Rad) and buffer consisting of 25 mM Tris/HCl, 86 mM glycine and 20% methanol. To avoid a nonspecific binding, the membrane was incubated in blocking buffer (5% non-fat dry milk, 0.1% Tween 20 in $1 \times$ TBS) for one h at room temperature. The incubation with a primary antibody recognizing cleaved anti-PARP fragment (mouse monoclonal Cat. Nr. 9544, Cell Signalling, Beverly, MA, USA) was performed overnight at 4 °C (diluted 1:1000). After washing with 0.1% Tween-20 in $1 \times$ TBS and incubation with the corresponding horseradish peroxidase-coupled secondary anti-rabbit antibody (Santa Cruz Biotechnology, Solna Sweden) (diluted 1:10,000) for 2 h at room temperature, the proteins were visualized with an Amersham ECL Western Blotting Detection Reagent (GE Healthcare Life Sciences, Little Chalfont, UK; Cat. Nr. RPN2106) accord-ing to the manufacturer's protocol. All membranes were incubated with the anti-extracellular-signal-regulated kinases 1/2 (anti-ERK1/2) (Santa Cruz Biotechnology, USA; Cat. Nr. sc-153) antibody to confirm equal protein loading. ERK1/2 were used as loading controls since no changes in total ERK1 and ERK2 expression was detected upon exposure of the cells to the different drugs [47,48].

2.5.5. Determination of DNA binding

The calf thymus ct-DNA was purchased from Sigma-Aldrich, dis-solved in Na-cacodylate buffer, $I = 0.05$ M, pH = 7, additionally sonicat-ed, and the solution was filtered through a 0.45 mm filter. The polynucleotide concentration was determined spectroscopically as the concentration of phosphates by $\varepsilon_{260\ nm} = 6600$ M^{-1} cm^{-1}. Circular di-chroism (CD) experiments were performed in quartz cuvette of 1 cm path length, by collecting CD spectrum of c(ct-DNA) $= 2.86 \times 10^{-6}$ M and subsequently adding small portions of compound to obtain ratios r[compound]/[ct-DNA] = 0.3, 0.5 and 0.7. The CD spectra of the mix-tures were collected after incubation times of 1 and 10 min to check any kinetic effect.

Thermal denaturation curves for the ct-DNA and its complexes with the studied compounds were determined in Na-cacodylate buffer, $I = 0.05$ M, pH = 7 by following the absorption change at 260 nm as a func-tion of temperature, as previously described [49,50]. The absorbance of the compound was subtracted from each curve and the absorbance scale was normalized. The measured T_m values are the midpoints of the transition curves determined from the maximum of the first derivative and checked graphically by the tangent method. The ΔT_m values were calculated subtracting T_m of the free nucleic acid from T_m of the complex. Every ΔT_m value here reported was an average of at least two measurements. The error in ΔT_m is ± 0.5 °C.

3. Results and discussion

3.1. Synthesis and characterization

The preparation of the 1,3-diaryltriazenes **1** was accomplished by a treatment of the appropriately substituted anilines with either sodium nitrite in hydrochloric acid or with isopentyl nitrite in dichloromethane as reported in the literature (see: 2.3. Reagents and materials). A subse-quent reaction of **1** with dinuclear p-cymene complex of ruthenium $[RuCl_2(\eta^6\text{-}p\text{-cymene})]_2$ in methanol and in the presence of triethylamine for 0.5 h afforded the triazenido-ruthenium complexes **2a–j** in good to excellent 61–91% yields (Scheme 1, Table 2). The exception to this was the 4-methoxyphenyl derivative **2k**, obtained in just 42% yield. The drop in the yield when going from **2a–j** to **2k** could be explained by the electron-releasing nature of the 4-methoxyphenyl substituents in the latter, decreasing the acidity of the triazene and making its reaction with the ruthenium precursor more sluggish (vide infra). All compounds **2** were isolated as coloured solids, stable in the air and in the solution of common organic solvents.

With the exception of **1a**, **1j**, and **1k**, the triazenes that had trifluoromethyl substituent in the structure were selected for this investigation. This was based on our previous observation that CF_3 substituent has the strongest influence on an antiproliferative activity of 1,3-diaryltriazenes as well as some of N-acyl derivatives to the tumor cells [18]. In the line with the fact that the fluorinated compounds could be more biologically active as their non-fluorinated analogues [51] is also our recent observation that CF_3 group has a distinct place in an anti-mycobacterial activity of 1,3-diaryltriazenes [14].

The structures of the complexes **2** were confirmed by the ^{1}H and ^{13}C NMR spectroscopy, a high-resolution time-of-flight mass spectrometry with an atmospheric pressure electrospray ionization (ESI HRMS) and microanalysis. It has been previously reported that in the carbon NMR spectra of 1,3-diaryltriazenes the resonances are broadened to the base-line [14,39], which could be accounted for by a dynamic triazene-triazene tautomeric exchange process that proceeds at the ^{13}C NMR time-scale. In contrast, the ^{13}C NMR resonances of the triazenido ligands in the compounds **2** show well defined line-shape. For both Ar groups in the triazenido ligand and the p-cymene ligand, one set of resonances were observed in the ^{1}H and ^{13}C NMR spectra indicating the symmetry of the complex **2**. The copies of the ^{1}H and ^{13}C NMR spectra are shown in the Supplementary Information. In ESI HRMS spectra the compounds **2** (measured in H_2O/CH_3CN) were characterized by the presence of [M–Cl]$^+$, whereas the ions for [M + H]$^+$ and [M–Cl + CH_3CN]$^+$ could also be observed. The complexes **2** were also characterized by determining melting points. The melting of the crystals is accompanied by a decom-position as evident from the TG/DSC measurements for the selected complexes **2e**, **f**, **g** (Fig. S1, Supplementary Information).

3.2. Crystal structures

The crystals, suitable for an X-ray analysis were obtained by a slow diffusion of petroleum ether into a solution of **2e** and **2h** in ethyl acetate. The structures of both compounds are displayed in Figs. 1 and 2, respec-tively. The structures of **2e** and **2h** exhibit a piano-stool geometry. The two nitrogen atoms of the triazenido bidentate chelating ligand, $\eta^6\text{-}p$-cymene ligand and chloride ion fulfil the coordination sphere around the ruthenium atom in both complexes. The compound **2e** crystalizes in orthorhombic *Pnma* space group with imposed mirror plane through Ru1, Cl1 and N2 atoms (Fig. 1) while **2h** crystalizes in monoclinic $P2_1/n$
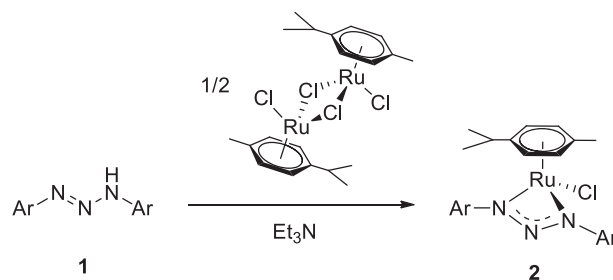
Scheme 1. Preparation of triazenido-ruthenium complexes **2**.

Table 2
A preparation of the triazenide complexes **2** and the key of the aromatic substituents (Scheme 1).

Triazene **1**	Ar—	Complex **2**	Yield[a]
1a		**2a**	80
1b	F₃C, F	**2b**	88
1c	CF₃, F	**2c**	74
1d	CF₃, Cl	**2d**	78
1e	F, F₃C	**2e**	61
1f	Cl, F	**2f**	83
1g	F₃C, Cl	**2g**	82
1h	F₃C, O₂N	**2h**	91
1i	F₃C, NC	**2i**	80
1j	I	**2j**	74
1k	H₃CO	**2k**	42

[a] Percent yield of the isolated pure product.

with the whole molecule in the asymmetric unit (Fig. 2). The Ru–N1 bond distances are from 2.080(4) to 2.109(2) Å and the bite angles N–Ru–N are from 101.7(4)° to 104.8(2)° in both complexes. All bond lengths and angles in the bidentate chelating system are within the range of the values described in literature for the related triazenido-ruthenium(II) complexes [23,25,27]. No significant hydrogen-bonding
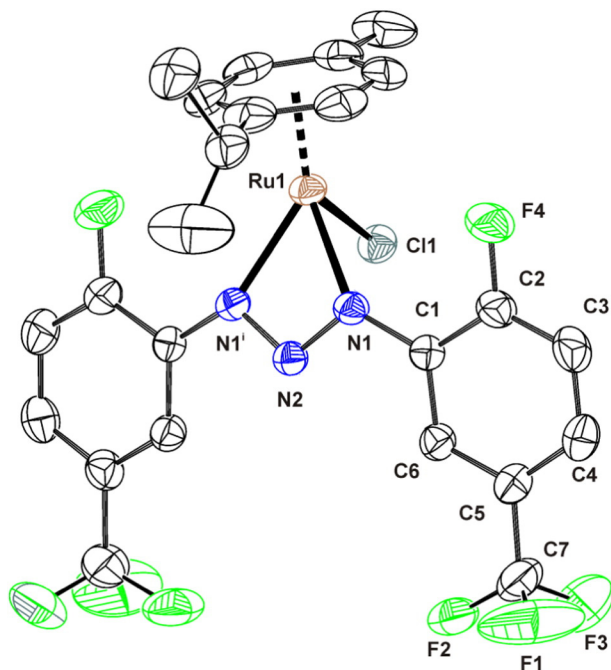

Fig. 1. ORTEP plot of **2e** with thermal ellipsoids at 30% probability level. Hydrogen atoms are omitted for clarity. Symmetry code: (i) (i) *x*, −1.5–*y*, *z*.
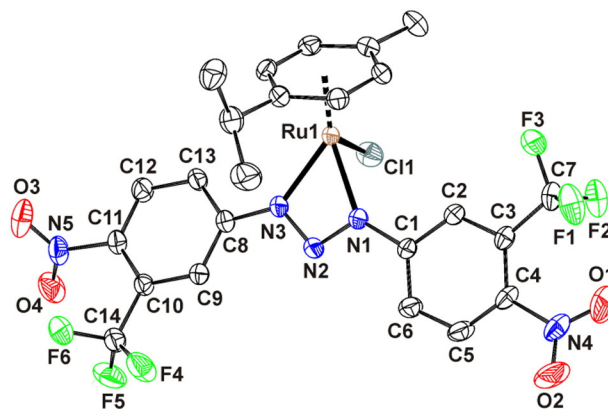

Fig. 2. ORTEP plot of **2h** with thermal ellipsoids at 30% probability level. Hydrogen atoms are omitted for clarity.

interactions could be observed in the crystal packing of **2e** and **2h**. The non-covalent C4–H4 · · · Cl1a [a: −x + 1, y + 1/2, −z + 2] and C12–H12C · · · Cl1b [b: x–1/2, −y–3/2, −z + 3/2] intermolecular contacts in **2e** connect the molecules into 3D supramolecular network (Fig. S2, Supplementary Information). In **2h** the molecules weakly interact each other through the C5–H5 · · · Cl1a [a: −x + 1, −y, −z], C19–H19 · · · F4b [b: −x + 1/2, −y + 1/2, z + 1/2], C17–H17 · · · O3c [c: x–1/2, −y + 1/2, z + 1/2] and C21–H21C · · · O4d [d: −x + 2, −y, −z] (Fig. S3, Supplementary Information) forming 3D supramolecular array. This 3D network in **2h** is further stabilized by the non-covalent C7–F1 · · · π interaction of 2.97 Å to one of the aromatic rings (C8–C13) in the crystal structure.

3.3. Cancer cell growth inhibition

A cytotoxic effect of the compounds **2** was first evaluated on a human cervical carcinoma HeLa cells, the cell model system that we found previously to be suitable for the screening of the new compounds [18,52]. As evident from Table 3, all compounds strongly inhibited the growth of the HeLa cells with IC$_{50}$ below 6 μM. The compound **2g** was the most cytotoxic with IC$_{50}$ of 0.103 ± 0.006 (after 72 h incubation), which is over 2000-times higher in comparison to the ruthenium precursor [RuCl$_2$(η^6-*p*-cymene)]$_2$ (IC$_{50}$ = 212.97 ± 2.14 [53]).

In general, the cytotoxicity of the triazenido-ruthenium complexes **2** was significantly increased as compared to the parental triazenes [16,18], confirming the occurrence of a synergistic effect. This is evident by comparison the data for the complexes **2c**, **2d**, **2g** and **2j** with those for the uncoordinated triazenes **1c**, **1d**, **1g** and **1j**, respectively (Table 3). The most pronounced difference was observed for the

Table 3
An antiproliferative activity of the compounds **2** towards the HeLa cells (IC$_{50}$ μM ± SD). IC$_{50}$ value after 72 h incubation.

2	IC$_{50}$ ± SD	**1**	IC$_{50}$
2a	1.543 ± 0.060		
2b	0.633 ± 0.038		
2c	0.230 ± 0.053	**1c**	10.86 ± 0.18
2d	5.923 ± 0.178	**1d**	62.2[a,b]
2e	0.603 ± 0.015		
2f	0.763 ± 0.099		
2g	0.103 ± 0.006	**1g**	58.38 ± 2.96[a]
2h	0.280 ± 0.035		
2i	0.770 ± 0.086		
2j	0.203 ± 0.025	**1j**	9.63 ± 0.06
2k	2.290 ± 0.184		

[a] Data from the literature [18].
[b] The highest concentration that could be evaluated, but with no influence on the cell survival.

Table 4
An antiproliferative activity of the selected ruthenium-triazenide complexes **2c**, **2g** and **2j** towards various tumor cell lines (IC_{50} μM + SD). IC_{50} value after 72 h incubation.

Cell line[a]	Compound		
	2c	**2g**	**2j**
HeLa	0.230 ± 0.053	0.103 ± 0.006	0.203 ± 0.025
HEp-2	0.226 ± 0.002	0.108 ± 0.015	0.180 ± 0.015
7 T	0.330 ± 0.037	0.109 ± 0.006	0.212 ± 0.020
HCT 116	0.249 ± 0.010	0.106 ± 0.009	0.180 ± 0.001
H460	0.300 ± 0.033	0.117 ± 0.004	0.208 ± 0.018
MDA-MB-435	0.297 ± 0.015	0.123 ± 0.018	0.329 ± 0.174

[a] HeLa = human cervical carcinoma cells; HEp-2 = laryngeal carcinoma cells; 7 T = drug-resistant HEp-2 subline; HCT-116 = colorectal carcinoma cells, H460 = lung adenocarcinoma cells; MDA-MB-435 = mammary carcinoma cells.

triazene **1g**, the activity of which increased upon a coordination to the ruthenium into **2g** by cca. 560-times.

From the triazenido-ruthenium complexes **2** we selected three highly active representatives **2c**, **2g** and **2j**, and examined their cytotoxicity against laryngeal carcinoma HEp-2 cells and their drug-resistant 7 T subline, colorectal carcinoma HCT-116 cells, lung adenocarcinoma H460 cells, and mammary carcinoma MDA-MB-435 cells. As evident from Table 4, the compound **2g** which was mostly cytotoxic for the Hela cells, strongly inhibited the growth of other tested cell lines as well. Modest differences in sensitivity between different cell lines were observed for **2c** and **2j**. The ratio in IC_{50} between the most sensitive and the most resistant tumor cell line was lower than 2 (for **2j**). For **2g** similar cytotoxicity against all cells examined was determined. In comparison to the other tumor cell lines, the H460 and MDA-MB-435 cells were more resistant to the selected complexes. It is important to note that the compounds **2g** and **2j** were similarly cytotoxic to the parental laryngeal carcinoma HEp-2 cells and to their drug-resistant 7 T subline, whereas the growth inhibitory effect of **2c** was more expressed on the parental than on the resistant 7 T cells.

3.4. Influence on the cell cycle

To get some insight into the molecular mechanism involved in the cytotoxicity of the triazenido-ruthenium complexes, the influence of **2g** on the progression of HeLa cells was monitored. This effect was investigated by a flow cytometry after 24 h and 48 h of the treatment with two concentrations that in MTT assay reduced the survival of the cells to 60 or 10% (survival fraction 0.6 and 0.1, respectively).

As shown in Table 5, the high dose of the compound **2g** caused a time and a dose dependent accumulation of the cells in the S phase of the cell cycle. It was accompanied by an increase of the cells present in the subG1 fraction, which represents the apoptotic cells.

3.5. Induction of an apoptosis

To further confirm that the compound **2g** indeed induces apoptosis, we explored the cleavage of the apoptosis marker PARP following the treatment of HeLa cells. As shown in Fig. 3., the compound **2g** induced a dose and time dependent cleavage of PARP. Even upon the treatment

Table 5
Effects of the compound **2g** on the cell cycle of HeLa cells.[a]

Survival fraction	24 h				48 h			
	G0/G1	S	G2M	subG1	G0/G1	S	G2M	subG1
0	58.58	20.54	20.88	7.33	60.39	27.79	11.82	5.97
0.6	61.91	24.43	13.66	10.06	57.44	34.77	7.79	6.24
0.1	29.68	58.73	11.59	14.53	31.37	55.52	13.11	22.16

[a] HeLa cells were treated for 24 h and 48 h with **2g**, stained with propidium iodide and analysed by flow cytometry. A cell cycle distribution was assessed as described in the Experimental section.
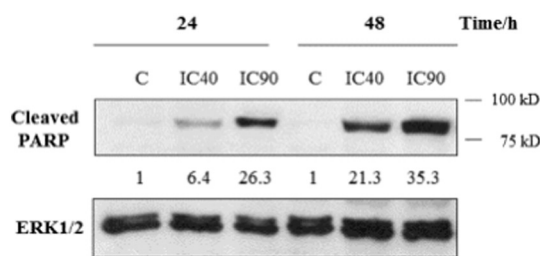

Fig. 3. A cleavage of PARP in HeLa cells upon 24 and 48 h treatment with two doses of **2g** which reduced the cell survival to 60% or 10% (IC_{40} and IC_{90}). Control cells were collected 24 and 48 h after the beginning of the treatment. ERK1/2 was used as a loading control. Precision Plus Protein™ All Blue Prestained Protein Standards (Bio-Rad, Cat. Nr. 1610373) is indicated in the figure. Representative data of three independent experiments are presented. Densitometric data are shown. Non-treated cells were set as 1.

with a lower dose and a shorter period of time, i.e. 24 h, the cleavage of PARP was observed.

3.6. DNA as possible target

To examine whether DNA is the target for the most cytotoxic compounds **2c**, **2g** and **2j**, as well as the corresponding uncoordinated triazenes **1c**, **1g** and **1j**, respectively, we studied their interaction with the double stranded DNA, namely calf thymus ct-DNA. All compounds and their metal complexes show an aggregation at rather low concentrations (starting from 4 to 9 μM). The study of interactions of the compounds with the ds-DNA (calf thymus; ct-DNA) was performed in the concentration range with linear absorbance-to-concentration dependence, i.e. the concentration in which the biological effect of complexes was determined (the IC_{50} value of all three selected complexes was below 0.35 μM). In a thermal denaturation experiment these compounds were mixed with the ct-DNA in a ratio $r_{[compound]/[ct-DNA]} = 0.3$ (pH 7, c(compound) < 3.5 μM), at which any DNA binding mode should give a measurable change in DNA melting point transition. However, none of the studied molecules stabilized the ct-DNA against thermal denaturation, indicating that at the biologically relevant conditions (pH 7, c(compound) = 10 μM) they do not form a stable non-covalent complex with the double stranded DNA (Fig. S4, Supplementary Information).

Furthermore, an addition of the ct-DNA caused changes in the UV–Vis spectra (Fig. S5, Supplementary Information) that could be assigned to the aggregation process (Fig. S4, Supplementary Information) particularly due to the noticeable increase of the baseline >450 nm, at which compounds do not absorb light. In the circular dichroism (CD) experiments CD bands of DNA (230–290 nm) did not change significantly upon the addition of any compound studied, which suggests that the DNA secondary structure is not affected by a small molecule binding [54,55]. Moreover, none of the studied compounds showed any specific CD band >300 nm upon mixing with DNA (Fig. S4, Supplementary Information), which usually appears for the achiral small molecules upon uniform binding to the DNA [56–58].

To conclude, thermal denaturation and CD and UV–Vis experiments suggest a non-specific aggregation of some compounds along DNA close to 0.1 mM concentrations of dye, with no significant impact on DNA properties (melting point, CD spectrum). Metal complexes did not show any interaction with DNA. Thus, the studied compounds do not show any biologically relevant interaction with ds-DNA.

4. Conclusions

Eleven new triazenido-ruthenium complexes were easily prepared by combining 1,3-diaryltriazenes with [RuCl₂(η⁶-p-cymene)]₂ in the presence of trimethylamine. All complexes exhibited high cytotoxic activity against several human carcinoma cells as well as against the drug-resistant subline. A selected complex **2g** induced time and dose

dependent accumulation of the cells in the S phase of the cell cycle and triggered apoptosis. Neither the triazenido-ruthenium complexes nor the uncoordinated 1,3-diaryltriazenes show biologically relevant interaction with ds-DNA. In the quest for a new anticancer drug candidate these promising preliminary results as well as the fact that no obvious structure-activity correlation could be found from the series of the examined compounds prompt for a screening of a larger set of triazenido-ruthenium complexes with subsequent molecular mechanism elucidation. Experiments are underway in our laboratories.

Acknowledgements

Appendix A. Supplementary data

Supplementary data to this article can be found online at http://dx.doi.org/10.1016/j.jinorgbio.2015.09.005

References

[1] B. Rosenberg, L. Van Camp, T. Krigas, Nature 205 (1965) 698–699.
[2] P. Heffeter, U. Jungwirth, M. Jakupec, C. Hartinger, M. Galanski, M. Elbling, M. Micksche, B. Keppler, W. Berger, Drug Resist. Updat. 11 (2008) 1–16.
[3] E. Wong, M.C. Giandomenico, Chem. Rev. 99 (1999) 2451–2466.
[4] M. Ohmichi, J. Hayakawa, K. Tasaka, H. Kurachi, Y. Murata, Trends Pharmacol. Sci. 26 (2005) 113–116.
[5] N.P.E. Barry, P.J. Sadler, Chem. Commun. 49 (2013) 5106–5131.
[6] K.J. Kilpin, P.J. Dyson, Chem. Sci. 4 (2013) 1410–1419.
[7] Y.K. Yan, M. Melchart, A. Habtemariam, P.J. Sadler, Chem. Commun. (2005) 4764–4776.
[8] P.J. Dyson, G. Sava, Dalton Trans. (2006) 1929–1933.
[9] G. Süss-Fink, Dalton Trans. 39 (2010) 1673–1688.
[10] R. Trondl, P. Heffeter, C.R. Kowol, M.A. Jakupec, W. Berger, B.K. Keppler, Chem. Sci. 5 (2014) 2925–2932.
[11] A.K. Singh, D.S. Pandey, Q. Xu, P. Braunstein, Coord. Chem. Rev. 270–271 (2014) 31–56.
[12] C.S. Allardyce, P.J. Dyson, Platin. Met. Rev. 45 (2001) 62–69.
[13] V. Brabec, O. Nováková, Drug Resist. Updat. 9 (2006) 111–122.
[14] D. Cappoen, J. Vajs, C. Uythethofken, A. Virag, V. Mathys, M. Kočevar, L. Verschaeve, M. Gazvoda, S. Polanc, K. Huygen, J. Košmrlj, Eur. J. Med. Chem. 77 (2014) 193–203.
[15] A.O. Ombaka, A.T. Muguna, J. Gichumbi, J. Environ. Chem. Ecotoxicol. 4 (2012) 133–136.
[16] D.B. Kimball, M.M. Haley, Angew. Chem. Int. Ed. 41 (2002) 3338–3351.
[17] M. Osmak, S. Polanc, T. Čimbora, A. Brozović, M. Kočevar, V. Majce, B. Alič, WO 2010/103338 A1.
[18] T. Čimbora-Zovko, A. Brozovic, I. Piantanida, G. Fritz, A. Virag, B. Alič, V. Majce, M. Kočevar, S. Polanc, M. Osmak, Eur. J. Med. Chem. 46 (2011) 2971–2983.
[19] G. Kiefer, T. Riedel, P.J. Dyson, R. Scopelliti, K. Severin, Angew. Chem. Int. Ed. 54 (2015) 302–305.
[20] F. Marchesi, M. Turriziani, G. Tortorelli, G. Avvisati, F. Torino, L. De Vecchis, Pharmacol. Res. 56 (2007) 275–287.
[21] L.K. Gediya, V.C.O. Njar, Expert Opin. Drug Discovery 4 (2009) 1099–1111.
[22] S. Patyar, A. Prakash, B. Medhi, J. Pharm. Pharmacol. 63 (2011) 459–471.
[23] C.F.B. da Silva, S. Schwarz, M.G. Mestres, S.T. López, J. Strähle, Z. Anorg. Allg. Chem. 630 (2004) 1919–1923.
[24] G. Albertin, S. Antoniutti, M. Bedin, J. Castro, S. Garcia-Fontán, Inorg. Chem. 45 (2006) 3816–3825.
[25] G. Albertin, S. Antoniutti, J. Castro, S. Paganelli, J. Organomet. Chem. 695 (2010) 2142–2152.
[26] N.S. Chowdhury, C. GuhaRoy, R.J. Butcher, S. Bhattacharya, Inorg. Chim. Acta 406 (2013) 20–26.
[27] F. Ehret, M. Bubrin, S. Záliš, W. Kaim, Angew. Chem. Int. Ed. 52 (2013) 4673–4675.
[28] J. Chu, X. Xiao-hua Xie, S. Yang, S. Zhan, Inorg. Chim. Acta 410 (2014) 191–194.
[29] J. Chu, Q. Lv, X. Xie, W. Li, S. Zhan, Transition Met. Chem. 38 (2013) 843–847.
[30] C. Tejel, M.A. Ciriano, G. Ríos-Moreno, I.T. Dobrinovitch, F.J. Lahoz, L.A. Oro, M. Parra-Hake, Inorg. Chem. 43 (2004) 4719–4726.
[31] J.M. Casas, B.E. Diosdado, L.R. Falvello, J. Forniés, A. Martín, Inorg. Chem. 44 (2005) 9444–9452.
[32] S.G. Alexander, M.L. Cole, C.M. Forsyth, S.K. Furfari, K. Konstas, Dalton Trans. (2009) 2326–2336.
[33] A.G.M. Barrett, M.R. Crimmin, M.S. Hill, P.B. Hitchcock, G. Kociok-Köhn, P.A. Procopiou, Inorg. Chem. 47 (2008) 7366–7376.
[34] W.H. Knoth, Inorg. Chem. 12 (1973) 38–44.
[35] Oxford Diffraction, CrysAlis PRO, Oxford Diffraction Ltd., Yarnton, England, 2009.
[36] Z. Otwinowsky, W. Minor, Methods Enzymol. 276 (1997) 307–326.
[37] A. Altomare, G. Cascarano, C. Giacovazzo, A. Guagliardi, J. Appl. Crystallogr. 26 (1993) 343–350.
[38] G.M. Sheldrick, Acta Crystallogr. A64 (2008) 112–122.
[39] B. Štefane, M. Kočevar, S. Polanc, J. Org. Chem. 62 (1997) 7165–7169.
[40] A. Khazaei, M. Kazem-Rostami, A.R. Moosavi-Zare, M. Bayat, S. Saednia, Synlett 23 (2012) 1893–1896.
[41] M. Osmak, L. Bizjak, B. Jernej, S. Kapitanovic, Mutat. Res. Lett. 347 (1995) 141–150.
[42] S. Rak, T. Cimbora-Zovko, G. Gajski, K. Dubravcic, A.M. Domijan, I. Delas, V. Garaj-Vrhovac, D. Batinic, J. Soric, M. Osmak, Toxicol. In Vitro 27 (2013) 523–532.
[43] A. Brozovic, L. Vuković, D.S. Polančac, I. Arany, B. Köberle, G. Fritz, Z. Fiket, D. Majhen, A. Ambriović-Ristov, M. Osmak, PLoS ONE 8 (2013), e76397 http://dx.doi.org/10.1371/journal.pone.0076397. eCollection 2013.
[44] A.F. Chambers, Cancer Res. 69 (2009) 5292–5293.
[45] G. Mickisch, S. Fajta, G. Keilhauer, E. Schlick, R. Tschada, P. Alken, Urol. Res. 18 (1990) 131–136.
[46] P.J. Duriez, G.M. Shah, Biochem. Cell Biol. 75 (1997) 337–349.
[47] A. Brozovic, G. Fritz, M. Christmann, J. Zisowsky, U. Jaehde, M. Osmak, B. Kaina, Int. J. Cancer 112 (2004) 974–985.
[48] C. Herraiz, F. Journe, Z. Abdel-Malek, G. Ghanem, C. Jimenez-Cervantes, J.C. Garcia-Borron, Mol. Endocrinol. 25 (2011) 138–156.
[49] J.-L. Mergny, L. Lacroix, Oligonucleotides 13 (2003) 515–537.
[50] I. Piantanida, B.S. Palm, P. Cudic, M. Zinic, H.-J. Schneider, Tetrahedron Lett. 60 (2004) 6225–6231.
[51] B.K. Park, N.R. Kitteringham, P.M. O'Neill, Annu. Rev. Pharmacol. Toxicol. 41 (2001) 443–470.
[52] B. Burja, T. Čimbora-Zovko, S. Tomić, T. Jelušić, M. Kočevar, S. Polanc, M. Osmak, Bioorg. Med. Chem. 18 (2010) 2375–2387.
[53] S. Grgurić-Šipka, I. Ivanović, G. Rakić, N. Todorović, N. Gligorijević, S. Radulović, V.B. Arion, B.K. Keppler, Ž. Lj Tešić, Eur. J. Med. Chem. 45 (2010) 1051–1058.
[54] J. Kypr, I. Kejnovská, D. Renčiuk, M. Vorlíčková, Nucl. Acids Res. 37 (2009) 1713–1725.
[55] A. Rodger, B. Nordén, Circular Dichroism and Linear Dichroism, Oxford University Press, New York, 1997.
[56] B. Norden, F. Tjerneld, Biopolymers 21 (1982) 1713–1734.
[57] R. Lyng, A. Rodger, B. Nordén, Biopolymers 31 (1991) 1709–1720.
[58] P.E. Schipper, B. Nordén, F. Tjerneld, Chem. Phys. Lett. 70 (1980) 17–21.